*Quantum Electronics* **36** (4) 369 – 375 (2006) 

PACS numbers: 32.80.Fb
DOI: 10.1070/QE2006v036n04ABEH013153

# Resonance laser-induced ionisation of sodium vapour taking radiative transfer into account

N.I. Kosarev, N.Ya. Shaparev

***Abstract*. The problem of ionisation of atomic sodium in the field of resonance laser radiation is numerically solved taking radiative transfer into account. Seed electrons are produced due to the mechanism of associative ionisation, then they gain energy in superelastic processes (collisions of the second kind) and initiate the avalanche ionisation of the medium by electron impact. We studied the effect of secondary radiation on the laser pulse propagation upon competition between the ionising and quenching electron collisions with excited atoms, on the kinetics of ionisation-induced vapour bleaching, and the plasma channel expansion in the form of a halo.**

***Keywords***: *spontaneous decay, excitation, de-excitation, absorption coefficient, source function, transparency, bleaching, radiative transfer, photoplasma.*

## 1. Introduction

The plasma produced when a gas experiences resonance laser irradiation (a photoplasma) has long and extensively been investigated. The first paper in this field was published by Lucatorto and McIlrath [1], who experimentally obtained a nearly complete ionisation of atomic sodium vapour with an initial density of $10^{15} - 10^{16}$ cm$^{-3}$ by pulsed laser irradiation at the wavelength of the resonance atomic transition ($\lambda = 589$ nm) with an intensity $J \leqslant 10^6$ W cm$^{-2}$. A review of the subsequent experimental research in this direction and the most significant potential applications of photoplasmas for practical purposes was presented in [2, 3] (see references therein). Unlike the conventional way of plasma production, which involves the inverse bremsstrahlung mechanism, the photoplasma is produced when the frequency of the laser field is close to the frequency of resonance atomic transition. The results of experiments of Ref. [1] were interpreted in Refs [4 – 6] on the basis of superelastic heating of electrons (collisions of the second kind), and the theoretical model which describes the formation of resonance plasma and is referred to as LIBORS in the literature [7 – 10] consists in the following. Initially the laser field saturates the resonance atomic transition. Then free (seed) electrons are produced in the medium due to associative ionisation. They gain energy in superelastic collisions by deactivating excited atoms, with the subsequent production of an electron avalanche resulting in complete ionisation of the gas.

The data calculated on the basis of the LIBORS model as well as of subsequent numerical models [11, 12] are in qualitative agreement with experimental data. Not enlarging on the advantages of the numerical algorithm constructed in Refs [11, 12] over the algorithm outlined in Refs [4 – 10], we only mention that the main factor underlying their limited nature is the method of taking into account the radiation transfer, which is based on the Biberman – Holstein approximation. As a matter of fact, in the optical resonance excitation of gas, the propagation of secondary radiation in the medium substantially changes its excitation kinetics. Furthermore, a detailed comparison of theoretical and experimental data is hindered by the nonlinear interaction of intense laser field with the medium, which may give rise to well-known concurrent effects. Among them is, for instance, the effect of spectral and spatial instability of the output laser intensity [3], which impedes measuring its magnitude.

Constructing the general model of photoplasma formation embracing a wide range of experimental parameters, like the medium density as well as the intensity and duration of laser pulses, is fraught with serious computational problems arising from the nonlinearity of the resultant systems of equations. However, on the basis of reviews [2, 3] it is valid to say that the propagation of resonance radiation in dense gaseous media is the key factor whose accurate inclusion in the numerical models under elaboration will permit bringing the calculated photoplasma parameters in proximity with the experimentally determined ones. The goal of the present work is numerical simulations of resonance laser-induced gas ionisation with the aim of studying the transfer of scattered radiation in the plasma formation and ionisation bleaching of the medium.

## 2. Collisional-radiative model

Laser radiation acts on the resonance $3S_{1/2} \leftrightarrow 3P_{1/2}$ transition in the sodium atom. The volume occupied by sodium vapour is assumed to be cylindrical in shape. When constructing a multilevel atomic model, one should bear in mind that the description of excitation and ionisation

**N.I. Kosarev** Siberian Juridical Institute, Ministry of Internal Affairs, Russian Federation, ul. Rokossovskogo 20, 660131 Krasnoyarsk, Russia; e-mail: kosarev_nikolai@mail.ru;
**N.Ya. Shaparev** Krasnoyarsk Scientific Centre, Russian Academy of Sciences, Presidium of the Krasnoyarsk Scientific Centre, Siberian Branch, Russian Academy of Sciences, Akademgorodok, 660036 Krasnoyarsk, Russia; e-mail: shaparev@icm.krasn.ru

Received 20 June 2005; revision received 22 December 2005
*Kvantovaya Elektronika* **36** (4) 369 – 375 (2006)
Translated by E.N.Ragozin

kinetics becomes progressively more accurate with increasing the number of states included. Highly excited levels play an important part in stepwise excitation and ionisation of the atoms by electron impact. However, at the stage of electron avalanche formation there simultaneously occurs, along with the excitation of the upper levels, their ionisation by electrons. Because the main objective of our work was to investigated the role of resonance radiation transfer in plasma formation and ionisation gas breaching, we restricted ourselves to an eight-level model of the sodium atom. Account was taken of the $3S_{1/2}$, $3P_{1/2}$, $3P_{3/2}$, 4S, 3D, 4P, and 5S levels and of the ionised state.

The kinetics of atomic level population will be described by balance equations. The following elementary processes were taken into account in the formation of state populations: photoexcitation, photoquenching and spontaneous decay; excitation and deexcitation by electron impact; associative ionisation of the $3P_{1/2}$ level and ionisation of atoms by electron impact; photo- and three-body recombination.

The equations describing the atomic state populations at a given point $r$ in the medium at the point in time $t$ are of the form

$$\frac{\partial N_1}{\partial t} = -P_{12}N_1 + P_{21}N_2 + \sum_{i=2}^{7} A_{i1}N_i$$

$$+ \sum_{i\neq 1}^{7}(K_{i1}N_i - K_{1i}N_1)N_e + R_1N_e^3 - S_1N_1N_e + F_1N_e^2, \qquad (1)$$

$$\frac{\partial N_2}{\partial t} = P_{12}N_1 - P_{21}N_2 + \sum_{i=3}^{7} A_{i1}N_i - A_{21}N_2$$

$$+ \sum_{i\neq 2}^{7}(K_{i2}N_i - K_{2i}N_2)N_e + R_2N_e^3 - S_2N_2N_e + F_2N_e^2 - \alpha_a N_2^2, \quad (2)$$

$$\frac{\partial N_m}{\partial t} = \sum_{i>m} A_{im}N_i - \sum_{i<m} A_{mi}N_m + \sum_{i\neq m}(K_{im}N_i - K_{mi}N_m)N_e$$

$$+ R_mN_e^3 - S_mN_mN_e + F_mN_e^2, \quad m = 3,4,5,6,7, \quad i = 1,2,\ldots,7, \qquad (3)$$

$$\frac{\partial N_e}{\partial t} = \sum_{i=1}^{7}(S_iN_iN_e - R_iN_e^3 - F_iN_e^2) + \alpha_a N_2^2, \qquad (4)$$

where $N_m(r,t)$ is the concentration of atoms in the $m$th state; $N_e(r,t)$ is the electron density; $A_{im}$ $(i > m)$ are the Einstein coefficients for spontaneous emission; $P_{12} = B_{12}J(r,t)$ and $P_{21} = B_{21}J(r,t) + A_{21}$ are the frequencies of radiative photoexcitation and photoquenching of the $3P_{1/2}$ excited level; $B_{12}$ and $B_{21}$ are the Einstein coefficients for absorption and stimulated emission; $J(r,t)$ is the solid-angle- and frequency-integrated radiation intensity at a point $r$ in the medium at the point in time $t$; $K_{mi}$ and $K_{im}$ are the level excitation and deexcitation rate coefficients due to electron collisions (the former was calculated in the Born approximation [13] and the latter employing detailed balance relations); $S_m$ are the electron collisional ionisation rate coefficients for the corresponding atomic states $m$ calculated by the Lotz formula [13]; $R_m$ are the three-body recombination rate coefficients calculated from the detailed balance relations; $F_m$ are the photorecombination rate coefficients determined by the method of Ref. [14]; and $\alpha_a$ is the rate coefficient for associative ionisation.

At the point in time $t = 0$ all atoms are in the ground state with a density $N_0$. The initial conditions for Eqns (1)–(3) are therefore as follows:

$$N_1(r,0) = N_0, \quad N_m(r,0) = 0, \quad m = 2,3,\ldots,7.$$

The equation for the electron temperature $T_e$ is of the form

$$\frac{\partial T_e}{\partial t} = \frac{2}{3}\sum_{i>k}^{7}(K_{ik}N_i - K_{ki}N_k)\Delta E_{ki} + \sum_{i=1}^{7}\left(\frac{2}{3}I_i + T_e\right)$$
$$\times(R_iN_e^2 - S_iN_i) - \frac{2}{3}H_{ea}\sum_{i=1}^{7}N_i - \frac{2}{3}H_{ei}N_e,$$

$$k = 1,2,\ldots,7, \qquad (5)$$

where $I_i$ are the ionisation potentials of the corresponding atomic levels; $\Delta E_{ki}$ is the difference between the energy levels $k$ and $i$; $H_{ea}$ и $H_{ei}$ are the energy transfer rates in elastic electron collisions with atoms and ions. Equations (4) and (5) were subject to the following initial conditions:

$$N_e(r,0) = 0, \quad T_e(r,0) = T_e^0.$$

Here, $T_e^0 \approx 0.05$ eV [12] is the initial temperature of the electrons produced due to associative ionisation.

The radiative transfer in Eqns (1)–(5) is taken into account with the help of coefficients $P_{12}$ and $P_{21}$, and $J(r,t)$ is defined by the expression

$$J(r,t) = \int_0^{2\pi} d\varphi \int_0^{\pi} \sin\theta\, d\theta \int_0^{\infty} \Phi(v)J(r,\theta,\varphi,v,t)dv. \qquad (6)$$

Here, $\Phi(v)$ is the absorption line profile, which was modelled by the Doppler frequency dependence:

$$\Phi(v) = \frac{1}{\sqrt{\pi}}\exp\left[-\frac{(v-v_0)^2}{\Delta v_D^2}\right];$$

$v_0$ is the central frequency of the spectral line; and $\Delta v_D$ is its Doppler width. The dependence of the radiation intensity $J(r,\theta,\varphi,v,t)$ on the frequency $(v)$, angular $(\theta,\varphi)$, and spatial $[r(x,y,z)]$ variables was determined from the transfer equation

$$\frac{\partial J(r,\theta,\varphi,v,t)}{\partial l} = \Phi(v)\chi_0(N_1,N_2)[S(N_1,N_2) - J(r,\theta,\varphi,v,t)]. \qquad (7)$$

We employed the stationary transfer equation, because the velocity of laser radiation propagation through the medium is much higher than the rate of variation of the medium parameters. Here, $dl$ is an infinitely small path increment of the photon travelling in an arbitrary direction $\boldsymbol{l}$; $\chi_0$ is the absorption coefficient at the line centre; and $S$ is the source function. In the case of complete redistribution over frequency and of the spherical photon scattering indicatrix, for $\chi_0$ and $S$ it is possible to write the expressions [15]

$$\chi_0(N_1, N_2) = \frac{c^2 A_{21} g_2}{8\pi \nu_0^2 g_1}\left(N_1 - \frac{g_1}{g_2}N_2\right),$$

$$S(N_1, N_2) = \frac{2h\nu_0^3 g_1}{c^2 g_2}\frac{N_2}{N_1 - (g_1/g_2)N_2}, \quad (8)$$

where $c$ is the velocity of light; $h$ is the Planck constant; $g_1$ and $g_2$ are the statistical weights of the states 1 and 2.

The laser beam had a symmetrical intensity distribution in the transverse section and was incident at right angle to the face of the cylinder with sodium vapour of height $H_0$. For the incident radiation, the boundary condition imposed on Eqn (7) at the left boundary ($z = -H_0/2$) is therefore of the form

$$J[r(z = -H_0/2), \theta, \varphi, \nu, t] = \begin{cases} 0, & \text{if} \quad \theta \neq 0, \\ J_{\text{las}}(R, \nu, t), & \text{if} \quad \theta = 0, \end{cases} \quad (9)$$

where $R$ is the radial coordinate at the input to the cylinder. Assuming that the incident radiation is absent at the right cylinder boundary ($z = H_0/2$), we obtain

$$J[r(z = H_0/2), \theta, \varphi, \nu, t] \quad \text{for} \quad \theta \geqslant 90, \quad (10)$$

where the $\theta$ variable is the angle between the scattered photon direction and the axis of symmetry $z$ of the cylinder. The time-and-frequency shape of the laser pulse was defined by the expression

$$J_{\text{las}}(R, \nu, t) = J_0 \frac{(\Delta\nu/2)^2}{(\nu - \nu_0)^2 + (\Delta\nu/2)^2}\frac{t}{\tau_p}\exp\left(1 - \frac{t}{\tau_p}\right)\mathscr{F}(R), \quad (11)$$

in which the function $\mathscr{F}(R)$ models the dependence of laser radiation intensity in the lateral beam section on the coordinate $R$; $\tau_p$ is the parameter which determines the pulse duration; and $\Delta\nu$ is the Lorentzian width of laser radiation spectrum.

Equations (1)–(11) are a closed system of integrodifferential equations. They were numerically solved on the basis of techniques elaborated in Refs [16–18] with the inclusion of radiation transfer in a cylindrically symmetric volume of the medium. Apart from the calculation of the population kinetics of multilevel atoms, the electron temperature and density, the algorithm enabled calculating the frequency-and-angular characteristics of the radiation scattered by sodium vapour for a set of spatial nodes at any given point in time. We outline the main results of the simulation of plasma formation kinetics.

## 3. Results of simulations

### 3.1 Ionisation bleaching of sodium vapour

Numerical simulations were performed for different initial densities of sodium atoms and laser radiation parameters (intensity and duration). We give the data for a uniform laser intensity distribution over the lateral beam section. The cylinder of height $H_0 = 1.0$ cm had a radius $R_0 = 0.5$ cm.

Figure 1 shows the temporal dependences of the electron temperature and density as well as of the populations of the ground and resonance levels for $\tau_p = 2$ μs, $\Delta\nu = 4\Delta\nu_D$, and $J_0 = 10^4$ W cm$^{-2}$. The initial atomic density was $N_0 = 3.56 \times 10^{14}$ cm$^{-3}$ for a vapour temperature of 562 K, for which the optical thickness of the medium along the cylinder axis was $\tau_0 = 2880$ at the central frequency of the resonance transition. The solid curves were obtained for the irradiated cylinder face at the axial point corresponding to the $z = -H_0/2$ coordinate and the dashed curves for the axial point on the shady cylinder face ($z = H_0/2$). The pulse intensity is high enough to ensure the laser-induced transparency of the volume under pumping, because the level populations reach close-to-saturated values ($N_1 \simeq N_2 \simeq 0.5N_0$) in a short time (no longer than 0.5 μs).

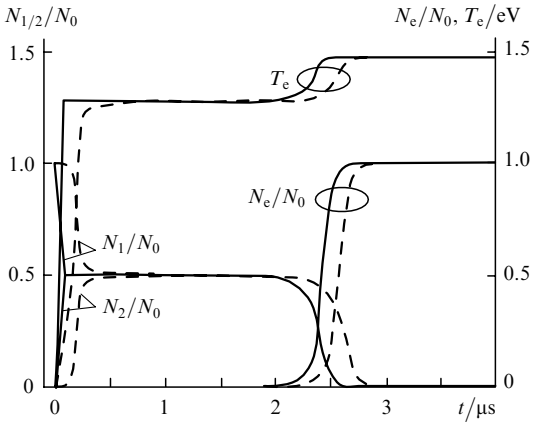


**Figure 1.** Time dependences of the electron density and temperature as well as of the atomic densities in the ground and excited ($3P_{1/2}$) states for $N_0 = 3.56 \times 10^{14}$ cm$^{-3}$, $\tau_p = 2$ μs, $\Delta\nu = 4\Delta\nu_D$, and $J_0 = 10^4$ W cm$^{-2}$. The solid curves correspond to the irradiated boundary and the dashed curves to the shady one.

The electrons, which emerge due to the associative mechanism, rapidly gain energy in superelastic collisions up to ~1.27 eV. This state with stationary level populations and electron energy exists until the initiation of the avalanche electron ionisation of atoms. As a result, the electron density increases sharply for $t \geqslant 2.0$ μs (Fig. 1). As the electron avalanche develops, the populations of the resonance (Fig. 1) as well as of all remaining excited levels decrease due to the lowering of the total density of the atoms. The electron temperature rises to 1.46 eV. The quasistationary value $T_e \approx 1.27$ eV is determined by the balance of direct and inverse transitions due to electron–atom collisions. The atomic density lowers in the transient state, and the electrons are heated when they quench the $3^2P_{1/2}$ excited level, whose population sustained by the laser radiation is significantly higher than the populations of all remaining excited levels. Next, the electron temperature reaches a new quasistationary value when all atoms are ionised.

Note that the $3^2P_{1/2}$ level population, the gaining of energy by electrons, and the ionisation of atoms at the shady cylinder face (the dashed curves in Fig. 1) are delayed. This is attributable to the absorption of laser radiation in its propagation from the irradiated side of the medium to the shady one.

Numerical investigations of the problem revealed the following features of resonance radiation transfer in the ionisation of sodium vapour. The escape of radiation through the lateral surface of the cylindrical volume is facilitated, resulting in a decrease of excited-atom density at the boundary. That is why the electron energy gained in superelastic collisions is lower at the boundaries than inside

the volume, where the radiation trapping provides a high excited-atom density. This is the reason why the electron collisional ionisation of atoms at the boundaries of the volume proceeds with a lower intensity [surfaces (*1*), (*2*) in Fig. 2]. Our calculations showed that the radiation is strongly absorbed in its propagation through the cylinder with sodium vapour for a lower pulse intensity ($J_0 \leqslant 10^3$ W cm$^{-2}$). In this case, the ionisation at the shady cylinder face, near the side surface, does not proceed at all. The radiation transfer therefore results in a nonuniform ionisation of atoms in the vapour volume, which is due to the absorption of laser radiation, the escape of photons from the medium, and the cooling of electrons at its boundaries.

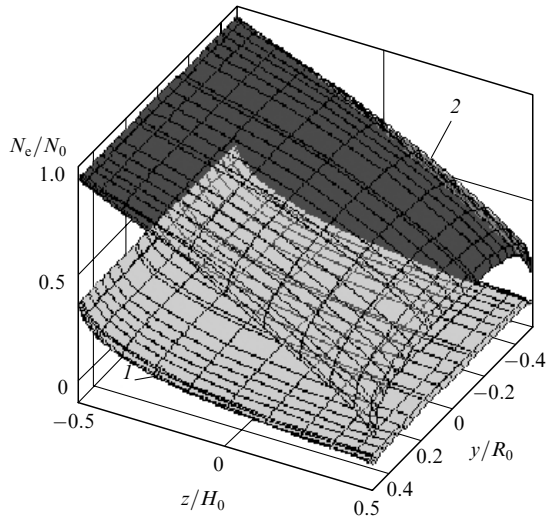


**Figure 2.** Spatial distribution of the electron density at the points in time $t = 2.4$ [surface (*1*)] and 2.56 μs [surface (*2*)]. The parameters of the model are the same as in Fig. 1.

Early in the transient process, when the electron avalanche is triggered, the medium becomes more opaque, because there appears an additional loss channel due to electron heating. This is testified by the data in Fig. 3. Plotted in Fig. 3 are the time dependences of the sodium vapour transmittance for laser radiation at different initial atom densities. One can see that the higher is $N_0$, the earlier is the onset of ionisation and the stronger is the medium opacity effect [curve (*1*)]. For a low atomic density, the onset of ionisation does not have time to occur whatsoever [curve (*4*)]. In this case, the lowering of transmittance is caused by the lowering of input pulse intensity for $t > \tau_p$. The opacity effect arises from the quenching of resonance levels by electrons.

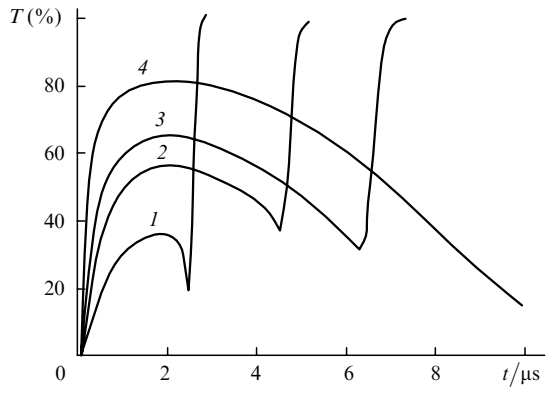


**Figure 3.** Time dependences of the transmittance $T$, which is the ratio between the frequency-integrated intensity of laser radiation transmitted through the cylinder with sodium and the incident radiation intensity, for the initial atomic densities $N_0 = 3.56 \times 10^{14}$ (*1*), $1.96 \times 10^{14}$ (*2*), $1.424 \times 10^{14}$ (*3*), and $6.76 \times 10^{13}$ cm$^{-3}$ (*4*). The pulse parameters are the same as in Fig. 1.

This effect was first predicted in paper [19], where it was shown that two regimes may be realised when a gas is subjected to resonance laser radiation. Initially, upon equalisation of the populations of resonance levels, seed electrons are produced, their energy spectrum becomes settled, and the subsequent buildup of electron density takes place due to the ionisation of atoms in collisions with electrons. With an increase in electron density, the absorption of laser radiation becomes stronger if the electron quenching rate is higher than the rate of ionising collisions. The second regime is realised in the case when the electron-impact ionisation rate exceeds the rate of quenching collisions, with the result that the medium becomes more transparent. The ionisation wave in the increase of laser radiation absorption is formed at the vapour surface under irradiation. Subsequently it travels inside the medium to additionally increase its transmittance. As this takes place, the gas may be completely ionised.

We draw attention to the following fact. The behaviour of curves (*1*)–(*3*) in Fig. 3 shows that the laser pulse breaks up into two subpulses at the vapour volume output. This is because the density of absorbing particles lowers due to the ionisation-induced bleaching of the medium and the absorption coefficient becomes smaller. Consequently, the dissipation of laser energy into the surrounding medium becomes smaller. This fact may turn out to be of the utmost significance for the transmission of laser energy through dense gases.

Figure 4 shows the laser intensity distributions in the $z$-coordinate of the cylinder at different points in time. Initially [curves (*1*) and (*2*)], the propagation of the pulse into the volume is associated with increase in the intensity of the pulse. The ionisation is not yet manifested. For $t > 1.6$ μs, an electron avalanche begins to develop, and the excited state is quenched by electron impact. The

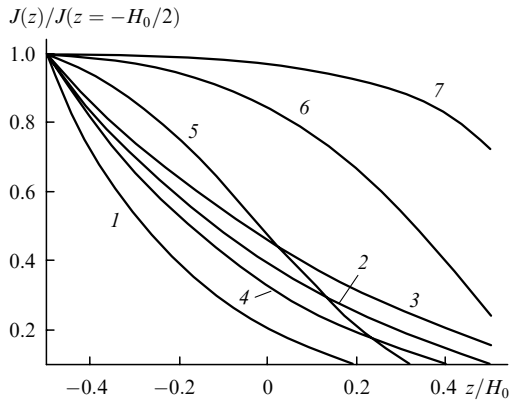


**Figure 4.** $z$-coordinate distribution of the relative intensity of laser radiation $J(z)/J(z = -H_0/2)$ at the points in time $t = 0.4$ (*1*), 0.8 (*2*), 1.6 (*3*), 2.32 (*4*), 2.4 (*5*), 2.48 (*6*), and 2.56 μs (*7*) for $N_0 = 3.56 \times 10^{14}$ cm$^{-3}$ and $J_0 = 5 \times 10^3$ W cm$^{-2}$.

medium becomes less transparent, the radiation intensity lowers at each section {the laser pulse front recedes to become closer to the boundary under irradiation [curve (*4*)]}. Subsequently, the degree of ionisation increases and the medium becomes more transparent again. As this takes place, the front of the laser pulse moves towards the shady cylinder face. Now it constitutes the front of ionisation bleaching. As this front propagates, in its fore part there forms a saturation zone, which is responsible for the development of electron collisional ionisation of atoms. The time dependence of pulse front velocity $V(t,z)$ was calculated numerically. When the front location in the $z$-axis changed by $\Delta z$ in a time $\Delta t$, the velocity $V(t,z)$ was defined as $\Delta z/\Delta t$. The excited-state quenching by electrons at the stage of electron avalanche formation leads to a backward motion of the front of the laser pulse, and $V(t,z)$ can therefore assume negative values as well. However, at the stage of avalanche ionisation it increases sharply and its maximum value $V_{\max}$ is as high as $6.0\times10^6$ cm s$^{-1}$. We now estimate the propagation velocity of the ionisation-bleached zone under the conditions of Ref. [19]:

$$V\approx\frac{L}{\tau_{\rm ion}},\quad \tau_{\rm ion}\approx[s'(N_1(0))]^{-1}\ln\frac{N_1(0)}{N'_{\rm e}},\qquad(12)$$

where $\tau_{\rm ion}$ is the characteristic time of vapour ionisation;

$$L\approx\left(1+\frac{g_1}{g_2}\right)\frac{J_0}{A_{21}N_1(0)}$$

is the length through which the radiation propagates in the saturation regime; $N'_{\rm e}=10^{-6}N_1(0)$ is the electron density determined by associative ionisation, whereby the dominant part in the ionisation of gas is played by electron impact; $s'=g_2s/(g_1+g_2)$; $s\approx1.2c_1(2/m_{\rm e})^{1/2}E^2/I_2$; $I_2$ is the ionisation potential of excited level 2; $E$ is the resonance radiation photon energy; $m_{\rm e}$ is the electron mass; the constant $c_1$ is determined by the cross section for resonance level excitation. We substitute in expression (12) the values of all parameters and constants for the transition of atomic sodium for $J_0=5\times10^3$ W cm$^{-2}$ and $N_0=3.56\times10^{14}$ cm$^{-3}$ to obtain $V=6.2\times10^6$ cm s$^{-1}$, which is close to the numerically simulated value of $V_{\max}$. If a higher laser intensity of $10^4$ W cm$^{-2}$ is taken, for the theoretical and numerically simulated velocity values we obtain $V=1.24\times10^7$ cm s$^{-1}$ and $V_{\max}=1.0\times10^7$ cm s$^{-1}$, respectively.

### 3.2 Plasma channel formation

Consider now the propagation of secondary radiation from the irradiated vapour zone to the periphery, where the laser radiation is missing. To do this, we simulated the action of a Gaussian beam on sodium vapour, and the function $\mathscr{F}(R)$ from expression (11) was of the form $\mathscr{F}(R)=\exp[-(R/R_{\rm las})^2]$, where $R_{\rm las}$ is the characteristic beam dimension. The following numerical parameters were used in the model: $R_{\rm las}<R_0$ ($R_{\rm las}=0.14$ cm, $R_0=0.5$ cm), $H_0/(2R_0)=1$, $J_0=5\times10^3$ W cm$^{-2}$, $\tau_{\rm p}=5$ μs, $N_0=3.56\times10^{13}$ cm$^{-3}$, $\tau_0=303$, the beam axis is coincident with the cylinder axis.

For these parameters of the model, the resonance radiation maintains the state of laser-induced transparency of the volume under pumping for a time interval $t\approx4\tau_{\rm p}$ and the excited-level population is close to the saturated one

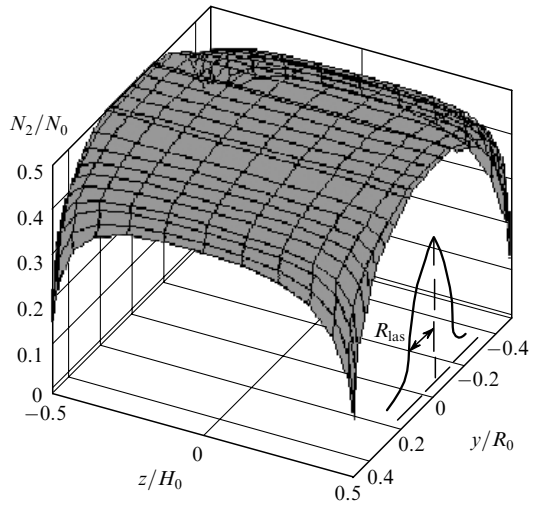


**Figure 5.** Spatial distribution of the excited-atom density at the point in time $t=\tau_{\rm p}$. The model parameters are described in the text.

(Fig. 5). Furthermore, the dimension of the zone with a high density of excited atoms is significantly greater than the characteristic beam radius $R_{\rm las}$. The expansion of the excited volume is caused by radial photon transfer from the region under pumping beyond its boundary. As the radial coordinate approaches the side cylinder surface, the excited-atom density lowers, which is related to the escape of photons from the medium. The ionisation gas bleaching in the laser beam zone begins for $t\geqslant4\tau_{\rm p}$, when the intensity of laser radiation is substantially lower.

When the ionisation zone propagates from the irradiated side of the medium to the shady one (Fig. 6a) there occurs a gradual bleaching of the entire volume under pumping (Fig. 6b). Moreover, the characteristic dimension of the ionised region is significantly greater than the laser beam dimension $R_{\rm las}$. This is attributable to the scattered radiation transfer in the radial direction to the periphery, with the effect that the density of excited atoms is high there. The free electrons produced outside the laser beam zone gain energy in superelastic collisions. Furthermore, when the electron avalanche is triggered in the beam zone, the electron collisional ionisation of atoms also develops in the peripheral region of the medium. Therefore, the radiation transfer is responsible for a strong photoexcitation of the medium beyond the Gaussian beam and for a significant expansion of the ionised volume, which manifests itself in the form of a halo.

## 4. Discussion of results

The gas ionisation mechanism which involves superelastic heating explains the experimentally observed features of photoplasma formation like the high efficiency of laser radiation conversion to the electron energy and ionisation; the full ionisation of the vapour pumped by laser radiation at relatively moderate intensities; the fast formation of plasma channels; and the superelastic electron heating, which furnishes the high conductivity of the plasma channels.

The results of numerical simulation of the plasma formation kinetics are in satisfactory agreement with theoretical calculations [19]. A detailed comparison with experimental data is hindered because, as noted in the

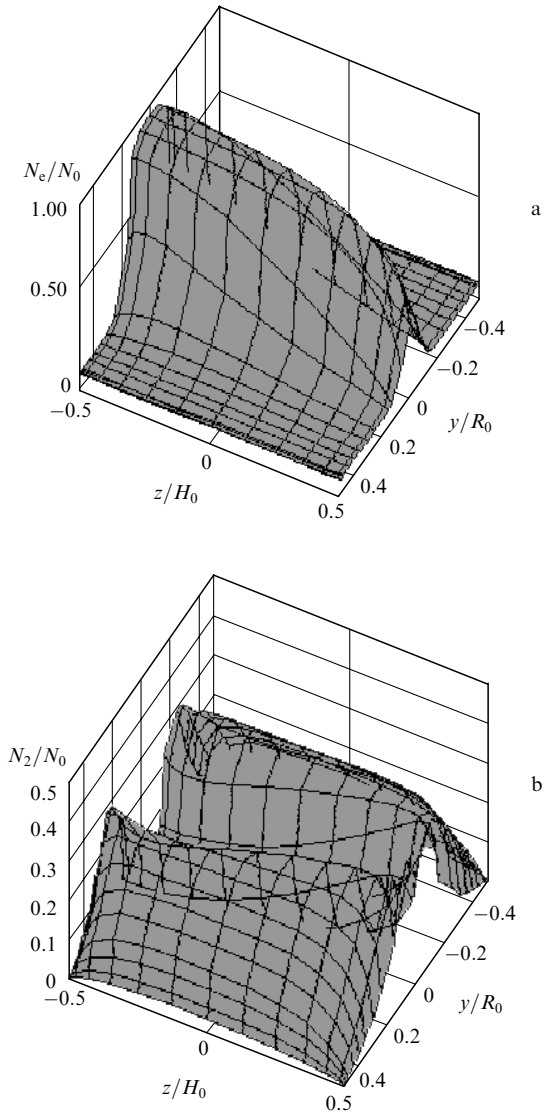


**Figure 6.** Spatial distribution of the electron density (a) and excited atoms (b) for $t = 30$ μs. The model parameters are the same as in Fig. 5.

Introduction, account should quite often be taken of concurrent nonlinear effects, which are responsible for the spectral and spatial instability of laser beams [3]. As a result, it is rather difficult to single out those experiments which are perfectly 'pure' in the sense that the radiative transfer has monopolistic effect on the excitation kinetics of a medium. The formulation of the problems involving an investigation of laser-induced resonance ionisation of metal vapours with a comprehensive treatment of the frequency-and-angular and spatial characteristics of the scattered resonance radiation are, as far as we know, absent in the literature. Nevertheless, an optical channel may quite often be the only way of gaining information when remote gas and plasma diagnostics is involved, and the inclusion of transfer is of significance for the interpretation of spectroscopic data.

In particular, the propagation of secondary radiation from the laser beam region to the medium periphery gives rise to a substantial broadening of the plasma channel because of the broadening of the saturation zone. These results indirectly bear out the assumptions of other authors concerning the problem of 'anomalous' fluorescence posed in Ref. [20]. Its discussion can be found, for instance, in Ref. [21] (see also references therein). According to Ref. [20], the fluorescence 'abnormality' is taken to mean the absence of intensity saturation of the secondary radiation scattered by sodium vapour ($\lambda = 589.6$ nm) with increase in laser intensity, despite the fact that the latter exceeded the saturation intensity by more than two orders of magnitude. Among the factors responsible for this intensity nonsaturability of the secondary radiation, as pointed out in Ref. [21] and demonstrated by Fig. 5, is the gradual saturation of the gaseous medium at the periphery, where there is no laser radiation. This is associated with the effect of vapour bleaching arising from the strong absorption of laser radiation due to the coincidence of its frequency with the resonance atomic line frequency in Ref. [20].

In the present work we investigated the possibility of calculating the characteristic time $\tau_{ion}$ for sodium vapour ionisation with the inclusion of secondary radiation. In the development of an avalanche ionisation of the atoms their density lowers, and the resonance line intensity will therefore decrease with time. Then, $\tau_{ion}$ can be determined numerically from the logarithmic damping decrement of the frequency-integrated intensity $J$ from the relation $J(t) = J_0 \exp(-t/\tau_{ion})$ under the assumption that $J(t)$ exhibits a single-exponential time dependence when t is large enough [2].

Note that in Ref. [22], where the 'opacity' effect was observed, the barium vapour was pumped by resonance laser radiation ($\lambda = 553.5$ nm) with a moderate intensity not exceeding $10^3$ W cm$^{-2}$. The barium atom has four metastable levels, which are coupled to each other and to the ground state via several excited states [17]. In the simulation of photoplasma formation for barium atoms, a rather large number of its excited states should therefore be included. The solution of this problem invites improvement and modification of the numerical algorithm.

## 5. Conclusions

The main results of our work are as follows.

We solved the problem of laser-induced resonance ionisation of sodium vapour ($\lambda = 589.6$ nm). A collisional-radiative model was constructed to describe transient excitation kinetics, the ionisation of multilevel sodium atoms, and radiation transfer. A numerical technique was elaborated for the solution of the resultant system of integrodifferential equations in the case of cylindrical geometry and large optical thicknesses of the medium. The algorithm permitted calculating the dynamics of the spatial distribution of atomic state populations, the dynamics of the electron density and temperature. To calculate the integrated intensity, the frequency-and-angular characteristics of the radiation scattered by sodium vapour were calculated on a three-dimensional grid for an arbitrary point in time employing the transfer equation.

The resonance laser radiation propagates as follows. Initially there occurs conventional laser-induced bleaching of the medium caused by absorption saturation. Subsequently this bleaching passes into additional bleaching (or 'opacity' which passes into bleaching). The medium 'opacity' is caused by an additional channel of energy losses arising from the superelastic quenching of resonance atoms and the bleaching is caused by a decrease of the density of these atoms due to their ionisation. The medium 'opacity' is

the reason why the laser pulse front recedes to the cylinder face under irradiation. The avalanche ionisation of the medium by electron impact also develops in the region. Subsequently, the ionisation wave propagates through the volume with an increasing velocity. As this takes place, at the output of the medium there occur two subpulses due to the decrease of the absorption coefficient. The lowering of laser energy absorbed in the course of ionisation of the atoms may be employed for the reduction of energy losses and a more efficient transfer of laser radiation energy. The absorption of laser radiation can also be lowered if its frequency is detuned from the central line frequency. In this case, the spatial and spectral beam shapes are retained and the degree of vapour ionisation remains high enough [3].

The radiation transfer results in a spatially nonuniform ionisation of sodium vapour. Inside the vapour volume, the excited-atom density, the electron temperature and density are higher due to radiation trapping. Near the medium boundaries, where the escape of photons is facilitated, the decay of the excited state leads to a lowering of the degree of ionisation.

The investigation of the dynamics of plasma channel formation revealed that the transfer of resonance radiation from the Gaussian beam zone to the periphery of the medium is responsible for its strong photoexcitation. Here, too, there develop associative ionisation of the atoms and an electron avalanche, which gives rise to a halo outside of the laser excitation region. The broadening of saturated vapour volume is an indirect proof that the self-absorption of resonance laser radiation is a factor accompanying the 'anomalous' fluorescence of metal vapours irradiated by laser beams. The characteristic vapour ionisation time can be calculated from the intensity damping decrement of their afterglow.

## References


1. Lucatorto T.B., McIlrath T.J. *Phys. Rev. Lett.*, **37** (7), 428 (1976).
2. Bezuglov N.N., Klyucharev A.N., Stasevich T. *Opt. Spektrosk.*, **77** (3), 342 (1994).
3. Leonov A.G., Starostin A.N., Chekhov D.I. *Zh. Eksp. Teor. Fiz.*, **111**, 1274 (1997).
4. Measures R.M. *J. Appl. Phys.*, **48**, 2673 (1977).
5. Shaparev N.Ya. *Abstr. Fourth Europhysics Sectional Conf. on Atomic and Molecular Physics of Ionized Gases* (Essen, Germany, 1978) Part 48.
6. Shaparev N.Ya. *Zh. Tekh. Fiz.*, **49**, 2223 (1979).
7. Measures R.M., Drewell N., Cardinal P. *J. Appl. Phys.*, **50** (4), 2662 (1979).
8. Measures R.M., Cardinal P.G., Schinn G.W. *J. Appl. Phys.*, **52** (3), 1269 (1981).
9. Measures R.M., Cardinal P.G. *Phys. Rev. A*, **23** (2), 804 (1981).
10. Measures R.M., Wong S.K., Cardinal P.G. *J. Appl. Phys.*, **53** (8), 5541 (1982).
11. Gavriluk A.P., Shaparev N.Ya. *Opt. Commun.*, **39** (6), 379 (1981).
12. Gavrilyuk A.P., Shaparev N.Ya. *Preprint No. 15* (Krasnoyarsk: Computation Centre, Siberian Branch of the USSR Academy of Sciences, 1986) Part 1.
13. Sobelman I.I., Vainshtein L.A., Yukov E.A. *Excitation of Atoms and Broadening of Spectral Lines* (Berlin: Springer-Verlag, 1981).
14. Sobelman I.I. *Atomic Spectra and Radiative Transitions* (Berlin: Springer-Verlag, 1979).
15. Mihalas D. *Stellar Atmospheres* (San Francisco: Freeman, 1978) Parts 1, 2.
16. Kosarev N.I., Shkedov I.M. *Opt. Atm. Okean.*, **6** (10), 1298 (1993).
17. Kosarev N.I., Shkedov I.M. *Opt. Atm. Okean.*, **12** (1), 30 (1999).
18. Kosarev N.I., Shkedov I.M. *Opt. Atm. Okean.*, **8** (12), 1752 (1995).
19. Shaparev N.Ya. *Zh. Eksp. Teor. Fiz.*, **80**, 957 (1981).
20. Salter J.M., Burgess D.D., Ebrahim N.A. *J. Phys. B: Atom. Molec. Phys.*, **12** (24), L759 (1979).
21. Leonov A.G., Panteleev A.A., Starostin A.N., et al. *Zh. Eksp. Teor. Fiz.*, **105**, 1536 (1994).
22. Bachor H.-A., Kock M. *J. Phys. B: Atom. Molec. Phys.*, **14**, 2793 (1981).